June 1993 Journal Article

RAPID DETERMINATION OF SATELLITE VISIBILITY PERIODS

PR: 9993
TA: LA
WU: BS

Salvatore Alfano, David Negron, Jr., Jennifer L. Moore

United States Air Force Academy
Colorado Springs, Colorado 80840

Phillips Laboratory
3550 Aberdeen Avenue, SE
Kirtland AFB, NM 87117-5776

PL-TR--93-1018

Published in Journal of the Astronautical Sciences, Vol. 40, No. 2, Apr-Jun 92, pp. 281-296.
Lt Col Alfano is presently assigned to PL/VTA, Kirtland AFB, NM 87117-5776.

This paper presents a numerical method to rapidly determine the rise-set times of satellite-satellite and satellite-ground station visibility periods, with the line-of-sight corrected for an oblate Earth. The algorithm uses a space curve modeling technique known as parabolic blending to construct the waveform of the visibility function, $\psi(t)$, versus time. The waveform is produced from either uniform or arbitrarily spaced abscissa points, from which rise-set times are obtained by extracting the real roots of a localized cubic polynomial. This algorithm works for all orbital eccentricities and perturbed satellite motion, provided the visibility function, $\psi(t)$, does not become discontinuous as it could from thrusting or deploying a tether. For this study, the rise-set *truth* table is constructed using a standard five second step-by-step integration with a linear interpolator to locate the exact crossing times. The simulation results from this algorithm are almost identical to those obtained by modeling satellites subject to first order secular perturbations caused by mass anomalies, but generated in considerably less time. Advantages of this numerical method include compact storage and ease of calculation, making it attractive for supporting ground-based and autonomous onboard satellite operations.

mathematical models, numerical methods and procedures, parabolas, visual surveillance, tracking, visibility, observation satellites (artificial)

17

Unclassified	Unclassified	Unclassified	SAR

The Journal of the Astronautical Sciences, Vol. 40, No. 2, April-June 1992, pp. 281-296

Rapid Determination of Satellite Visibility Periods

Salvatore Alfano,[1] David Negron, Jr.,[2] and Jennifer L. Moore[3]

Abstract

This paper presents a numerical method to rapidly determine the rise-set times of satellite-satellite and satellite-ground station visibility periods, with the line-of-sight corrected for an oblate Earth. The algorithm uses a space curve modeling technique known as parabolic blending to construct the waveform of the visibility function, $\psi(t)$, versus time. The waveform is produced from either uniform or arbitrarily spaced abscissa points, from which rise-set times are obtained by extracting the real roots of a localized cubic polynomial. This algorithm works for all orbital eccentricities and perturbed satellite motion, provided the visibility function, $\psi(t)$, does not become discontinous as it could from thrusting or deploying a tether. For this study, the rise-set *truth* table is constructed using a brute force step-by-step integration with five second intervals; a linear interpolator is then used to locate the crossing times. The simulation results from this algorithm are almost identical to those obtained by modeling satellites subject to first order secular perturbations caused by mass anomalies, with a 95% decrease in computation time over the brute force method. Advantages of this numerical method include compact storage and ease of calculation, making it attractive for supporting ground-based and autonomous onboard satellite operations.

Introduction

The traditional rise-set problem consists of determining the viewing periods of a satellite versus an Earth-fixed tracking station. With few satellites aloft, the early days of satellite operations consisted of establishing communications whenever a vehicle entered the ground station's visibility window. With a tabulation of rise-set times, satellite operators were prepared to transmit and receive data from the vehicle. These operations have changed significantly. Satellites are now deployed with mission effectiveness highly reliant on spaceborne tracking and crosslink communications. Manufacturers currently design satellites to be

[1]Associate Professor, Astrodynamics Division Chief, Department of Astronautics, United States Air Force Academy, DFAS, CO 80840.
[2]Assistant Professor, Astrodynamics Division, Department of Astronautics, United States Air Force Academy, DFAS, CO 80840.
[3]Space Operations Officer, Air Force Space Command.

operator interactive even when outside the visibility window of a ground station. Mission designers are concerned with how a satellite deployment strategy *loads* a ground station, as well as the frequency and duration of high conflicts. This is a key orbit-design issue because competition for ground station support is usually resolved with the highest priority satellite awarded support. Also, as the satellite altitude decreases the opportunities to track or communicate with the vehicle from a ground station become more restricted, further complicating the satellite scheduling process. These issues call for a computationally efficient routine to determine satellite-satellite and satellite-ground station visibility periods that is capable of processing all orbit types.

Satellite-satellite and satellite-ground station visibility periods are typically determined by evaluating Earth centered inertial position vectors of the two objects of interest. An orbital simulation is advanced in time by some small time increment, Δt, and a visibility check is performed at each step. One drawback to this method is computation time, especially when modeling many perturbations and processing several vehicles. An additional disadvantage can be the imprecision of the satellite rise-set determination resulting from the simulation step size Δt. Escobal [1] proposed a faster method to solve the satellite versus Earth-fixed tracking station problem by developing a closed-form solution for the visibility periods about an oblate Earth. Escobal transforms the satellite and tracking station geometry into a single transcendental equation as a function of eccentric anomaly. Numerical methods are then used to find the rise and set anomalies, if they exist. More recently, Lawton [2] developed a method to solve for satellite-satellite and satellite-ground station visibility periods (hereafter called the satellite rise-set problem) for vehicles in circular or near circular orbits by approximating the visibility function, $\psi(t)$, with a Fourier series. Exploiting the sinusoidal nature of the visibility curve generated by satellites with orbital eccentricities less than 0.1, he determines the local periodicity of this curve and then uses a numerical search to locate rise-set times. This method works well for low eccentricity orbits, but fails for more elliptical orbits because the visibility waveform becomes aperiodic. This paper presents a highly accurate, computationally efficient, numerical method to solve the satellite rise-set problem for all orbit types.

The Visibility Function

Let $\mathbf{r}_1$ and $\mathbf{r}_2$ be the Earth centered inertial position vectors of the two objects of interest at time t. Define the visibility function, $\psi(t)$, as

$$\psi(t) = \cos^{-1}\left\{\frac{R_\oplus + h}{|\mathbf{r}_1|}\right\} + \cos^{-1}\left\{\frac{R_\oplus + h}{|\mathbf{r}_2|}\right\} - \cos^{-1}\left\{\frac{\mathbf{r}_1 \cdot \mathbf{r}_2}{|\mathbf{r}_1|\,|\mathbf{r}_2|}\right\}, \tag{1}$$

where

$$\psi(t)\begin{cases} < 0 & \text{no visibility} \\ = 0 & \text{rise or set condition} \\ > 0 & \text{visibility exists.} \end{cases}$$

The fundamental unit of length is one Earth radii ($R_\oplus$) and a bias factor (h) accounts for the impact of another parameter, such as atmospheric interference.

Figure 1 shows the geometry of the visibility function, with the position vectors forced to reside in an Earth-tangent plane. This function is determined by comparing the angle between $\mathbf{r}_1$ and $\mathbf{r}_2$ to the angles formed from the line-of-sight tangent to the spherical surface at $R_\oplus + h$. To correct for oblateness, rescale the $\hat{\mathbf{k}}$ component of $\mathbf{r}_1$ and $\mathbf{r}_2$ by $1/\sqrt{1 - e_e^2}$, where e_e is the eccentricity of the Earth ellipsoid. Tabulating $\psi(t)$ at 250 second intervals,[1] the curve fitting is accomplished by approximating the waveform with localized cubic polynomials. Anytime the visibility curve transitions the horizontal axis, the time of crossing is determined by the corresponding polynomial root. An advantage of this fitting process is the localized curve model, where the curve must be continuous, but need not conform to a sinusoidal-like function. By inspection, the arguments in equation (1) are between -1 and 1, inclusive, making the inverse cosine function continuous. Thus, by the summing property of functions, $\psi(t)$ is also continuous.

Curve Fitting

There are many techniques available to accomplish curve fitting. To alleviate the problems associated with restrictive sinusoidal fits or high-order generalized polynomials, a computer graphics technique known as parabolic blending is used. This method was originally developed by A.W. Overhauser [3] and then refined by Brewer and Anderson [4].

A series of polynomial functions, each defined by three data points, are used to approximate the visibility waveform. Curve fitting by parabolic blending uses four consecutive points to create two second order curve functions. The first curve is created from the first three data points with the latter three points defining the second curve. As shown in Fig. 2, the curve segments passing through the central points are then linearly blended into a single third order

[1]The interval at which $\psi(t)$ is tabulated is designer chosen, but the reader is cautioned against choosing a step too large. As the interval is increased, accuracy of the curve fit is decreased, possibly resulting in *missed* crossing times for rapidly varying data.

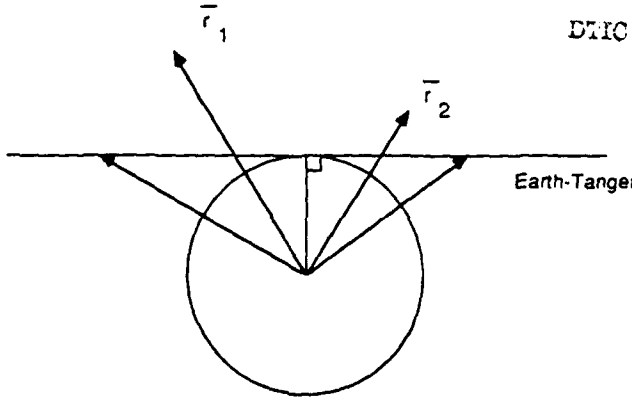

FIG. 1. Geometry to Compute the Visibility Function.

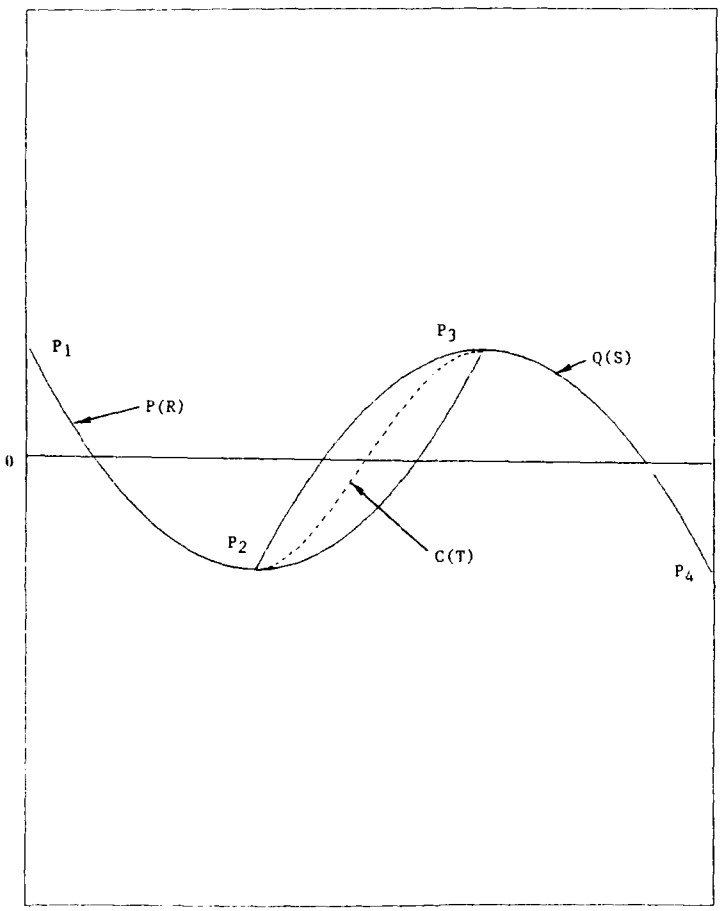

FIG. 2. Nomenclature for Parabolic Blending.

polynomial. The equation to accomplish the blending is chosen such that the blended curve matches the slope of the first parabola at the second point and also matches the slope of the second parabola at the third point. This blending process is repeated until the data set is exhausted, resulting in a first order continuous curve created from numerous localized parabolas.

Parabolic blending is accomplished by using four consecutive points ($\rho_1, \rho_2, \rho_3, \rho_4$), as shown in Fig. 2. The first parabola, P, ranges from the first point to the third point as a function of the unitized parameter R. The second parabola, Q, ranges from the second point to the fourth point as a function of the unitized parameter S. The C curve, ranging between the second and third points, weights the P and Q curves through the linear blending function

$$C(T) = (1 - T)\,P(R) + T\,Q(S) \qquad 0 \leq T \leq 1. \tag{2}$$

Rise and set times occur whenever the visibility function changes sign. To determine these times of occurrence, the C curve is reformulated as a cubic polynomial in T, and its roots solved with $C(T)$ set to zero. The roots are ignored if they are imaginary, repeating, or outside the range of T. Any remaining roots designate the unitized rise and set times in the specified interval $[\rho_2, \rho_3)$. Thus, the cubic equation for $C(T)$ given four consecutive points $(\rho_1, \rho_2, \rho_3, \rho_4)$ is given by

$$C(T) = \alpha_3 T^3 + \alpha_2 T^2 + \alpha_1 T + \alpha_0, \tag{3}$$

where

$$\alpha_0 = \rho_2 \tag{4}$$

$$\alpha_1 = -\frac{1}{2}\rho_1 + \frac{1}{2}\rho_3 \tag{5}$$

$$\alpha_2 = \rho_1 - \frac{5}{2}\rho_2 + 2\rho_3 - \frac{1}{2}\rho_4 \tag{6}$$

$$\alpha_3 = -\frac{1}{2}\rho_1 + \frac{3}{2}\rho_2 - \frac{3}{2}\rho_3 + \frac{1}{2}\rho_4. \tag{7}$$

By choosing four consecutive ψ values from a reference file, the α_ψ coefficients are easily computed for the polynomial equation $C_\psi(T)$ and then used to solve for the real unique root(s), T_{ROOT}. If the root(s) is within bounds, the α_i coefficients are computed using the times that correspond to the ψ values. This resulting $C_i(T)$ equation yields the rise or set time associated with T_{ROOT}. Figure 3 shows a typical mapping from the visibility to the time waveform, with equally spaced data points producing a linear waveform for time. When near the beginning or end of the reference file, blending is accomplished by repeating the endpoints. Appendix A presents a complete algorithm to generate a rise-set table for a computer routine.

Simulation Results

The rise-set values obtained by this method are compared to those from a standard general perturbations step-by-step integration. For this study the two objects of interest, be it satellites or satellite and ground station, are advanced in time at five second intervals as was done by Lawton [2]. At each integration step a visibility check is performed with a linear interpolation used to determine the rise-set times. These results, which serve as the *truth*, are obtained by influencing the satellite(s) by first order secular rates caused by mass anomalies [5] listed below.

$$\bar{n} = n_0\left[1 + \frac{3}{2}J_2\frac{\sqrt{1-e^2}}{p^2}\left(1 - \frac{3}{2}\sin^2 i\right)\right] \tag{8}$$

$$\dot{\Omega} = -\left(\frac{3}{2}\frac{J_2}{p^2}\cos i\right)\bar{n} \tag{9}$$

$$\dot{\omega} = \left(\frac{3}{2}\frac{J_2}{p^2}\left[2 - \frac{5}{2}\sin^2 i\right]\right)\bar{n}, \tag{10}$$

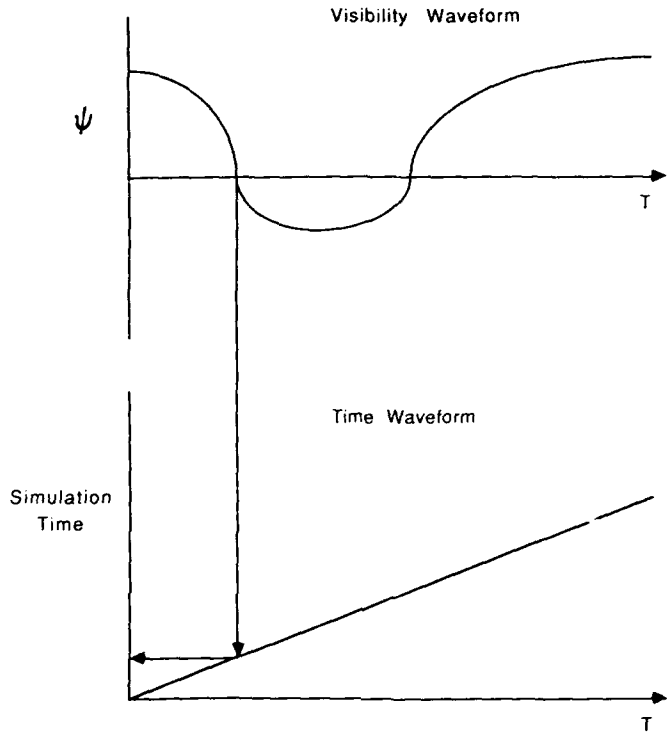

FIG. 3. A Typical Visibility and Time Waveform Pair.

where $\bar{n}$ is the anomalistic mean motion, n_0 is the mean motion at epoch, J_2 is the second harmonic coefficient, p is the semi-latus rectum, e is the eccentricity, i is inclination, $\dot{\Omega}$ is the nodal rate, and $\dot{\omega}$ is the periapsis rate. For simulation results involving an Earth-fixed tracking station, the site is initialized at the principal axis and its future position given by [5]

$$x = G_1 \cos(\phi) \cos(\theta) \tag{11}$$

$$y = G_1 \cos(\phi) \sin(\theta) \tag{12}$$

$$z = G_2 \sin(\phi), \tag{13}$$

where ϕ is the station geodetic latitude and θ is the local sidereal angle, and

$$G_1 = \frac{1}{\sqrt{1 - e_e^2 \sin^2(\phi)}} + H \tag{14}$$

$$G_2 = \frac{1 - e_e^2}{\sqrt{1 - e_e^2 \sin^2(\phi)}} + H, \tag{15}$$

where e_e is the eccentricity of the Earth ellipsoid and H is the altitude deviation from the ellipsoid.

Classical orbital elements from the United States Space Command satellite catalogue are used as test data for this study, and are listed in Table 1. These elements were obtained by sorting the catalogue, which includes thousands of satellites, by orbital eccentricity, mean motion, and inclination. The satellites with the least and greatest eccentricity, along with the satellites having the greatest mean motion and inclination, are used as test data. Also, for this study, the Earth-fixed tracking station is placed at the United States Air Force Academy and is initialized at the vernal equinox. Thus, the station coordinates become 104° west longitude, 39° geodetic latitude, with 2.9 km deviation above the ellipsoid.

Tables 2 through 8 show the rise-set times for a one day simulation using the pairs of permutations created from the Space Command orbital elements listed in Table 1. The extensive results, representing the extremes of the tracked satellite population, demonstrate the accuracy of the curve fit for the specified time interval. Along with each rise-set table a visibility waveform created by parabolically blending the 250-second spaced data points is shown in Figs. 4 through 9.

TABLE 1. Classical Orbital Elements ($\omega = \Omega = MA = 0°$)

Satellite	N(rev/solar day)	e	i(deg)
1	1.00272141	.0000032	0.0956
2	0.24891961	.9363060	64.9874
3	16.09769232	.0078742	82.8709
4	13.84150848	.0048964	144.6414

TABLE 2. One Day Rise-Set Summary for Satellite #1 vs Satellite #3

Parabolic Blending		Angles Simulation		Absolute Difference	
Rise	Set	Rise	Set	Rise	Set
	1450.2		1450.2		0.0
3965.4	6889.5	3965.4	6889.6	0.0	0.1
9371.1	12399.3	9371.1	12399.4	0.0	0.1
14774.0	18420.0	14773.8	18419.9	0.2	0.1
20218.0	25546.7	20218.2	25546.5	0.2	0.2
27789.3	30949.7	27789.1	30949.9	0.2	0.2
33360.0	36352.2	33359.9	36352.1	0.1	0.1
38814.5	41760.1	38814.4	41760.1	0.1	0.0
44235.7	47181.6	44235.7	47181.6	0.0	0.0
49643.3	52636.5	49643.4	52636.6	0.1	0.1
55045.1	58209.9	55044.9	58210.2	0.2	0.3
60445.5	65807.0	60445.8	65806.8	0.3	0.2
67619.8	71227.2	67620.0	71227.4	0.2	0.2
73604.4	76628.6	73604.2	76628.6	0.2	0.0
79111.0	82034.0	79110.9	82033.9	0.1	0.1
84549.4	———	84549.4	———	0.0	—

TABLE 3. One Day Rise-Set Summary for Satellite #1 vs Satellite #4

Parabolic Blending		Angles Simulation		Absolute Difference	
Rise	Set	Rise	Set	Rise	Set
— — —	1805.8	— — — —	1805.8	—	0.0
4071.1	7692.5	4071.1	7692.6	0.0	0.1
9900.8	13547.3	9900.7	13547.3	0.1	0.0
15662.3	19334.9	15662.3	19334.9	0.0	0.0
21382.3	25066.5	21382.2	25066.4	0.1	0.1
27134.5	30810.5	27134.4	30810.5	0.1	0.0
32961.4	36617.7	32961.5	36617.7	0.1	0.0
38842.9	42484.0	38842.8	42484.0	0.1	0.0
44737.1	48377.8	44737.1	48377.8	0.0	0.0
50604.7	54259.7	50604.7	54259.7	0.0	0.0
56413.5	60087.9	56413.5	60087.9	0.0	0.0
62158.3	65841.0	62158.3	65841.0	0.0	0.0
67888.4	71560.2	67888.3	71560.1	0.1	0.1
73673.4	77319.7	73673.4	77319.7	0.0	0.0
79526.4	83147.8	79526.3	83147.8	0.1	0.0
85412.6		85412.6		0.0	

TABLE 4. One Day Rise-Set Summary for Satellite #2 vs Satellite #3

Parabolic Blending		Angles Simulation		Absolute Difference	
Rise	Set	Rise	Set	Rise	Set
	2997.7		2997.7		0.0
5931.1	8939.9	5931.1	8939.9	0.0	0.0
11435.4	14472.8	11435.4	14472.8	0.0	0.0
16877.8	19934.3	16877.8	19934.4	0.0	0.1
22297.7	25367.3	22297.7	25367.3	0.0	0.0
27706.2	30785.3	27706.3	30785.3	0.1	0.0
33108.0	36194.1	33108.0	36194.1	0.0	0.0
38505.3	41597.0	38505.3	41597.0	0.0	0.0
43899.5	46995.6	43899.5	46995.6	0.0	0.0
49291.3	52391.1	49291.3	52391.1	0.0	0.0
54681.3	57784.3	54681.3	57784.3	0.0	0.0
60069.9	63175.5	60069.9	63175.5	0.0	0.0
65457.4	68565.3	65457.4	68565.3	0.0	0.0
70844.0	73953.8	70844.0	73953.8	0.0	0.0
76229.8	79341.4	76229.9	79341.4	0.1	0.0
81615.1	84728.0	81615.1	84728.0	0.0	0.0

The time step of 250 seconds was chosen to ensure accuracy when examining any satellite in the United States Space Command catalogue; this interval can be increased for low eccentricity orbits. The user is advised to select a time step and run several test orbits to determine if the accuracy is adequate for mission requirements. As mentioned, this routine works for an oblate Earth as well, with Tables 7 and 8 showing these results. In particular, Tables 4 and 7 are created

TABLE 5. One Day Rise-Set Summary for Satellite #2 vs Satellite #4

Parabolic Blending		Angles Simulation		Absolute Difference	
Rise	Set	Rise	Set	Rise	Set
	4931.7		4931.9		0.2
7111.7	11272.6	7111.6	11272.5	0.1	0.1
13412.0	17536.5	13412.0	17536.5	0.0	0.0
19673.3	23787.2	19673.3	23787.1	0.0	0.1
25923.6	30032.6	25923.6	30032.6	0.0	0.0
32169.1	36275.3	32169.1	36275.3	0.0	0.0
38412.0	42516.4	38411.9	42516.3	0.1	0.1
44653.1	48756.3	44653.1	48756.3	0.0	0.0
50893.2	54995.5	50893.2	54995.5	0.0	0.0
57132.5	61234.1	57132.5	61234.2	0.0	0.1
63371.3	67472.3	63371.2	67472.3	0.1	0.0
69609.6	73710.1	69609.5	73710.2	0.1	0.1
75847.6	79947.7	75847.5	79947.7	0.1	0.0
82085.3	86185.2	82085.2	86185.1	0.1	0.1

TABLE 6. One Day Rise-Set Summary for Satellite #3 vs Satellite #4

Parabolic Blending		Angles Simulation		Absolute Difference	
Rise	Set	Rise	Set	Rise	Set
	728.0		728.3		0.3
2145.0	3508.9	2145.8	3508.6	0.8	0.3
34217.0	35246.6	34218.2	35246.7	1.2	0.1
36889.2	38274.5	36889.6	38274.1	0.4	0.4
39624.2	41174.8	39624.3	41175.0	0.1	0.2
42840.0	43670.7	42839.6	43671.6	0.4	0.9
72091.7	72474.1	72088.1	72476.2	3.6	2.1
74570.3	75735.8	74570.2	75736.2	0.1	0.4
77179.5	78783.7	77179.9	78783.4	0.4	0.3
80215.3	81418.2	80216.3	81418.1	1.0	0.1
83415.2	83937.6	83416.4	83940.2	1.2	2.6

from the same satellite pair, but Table 7 includes the line-of-sight between the satellites being corrected for an oblate Earth. An oblate Earth will yield earlier rise times and later set times when the line-of-sight vector does not cross the equatorial plane, a fact typically omitted in the published literature. The rise-set summary for satellite #1 versus #2 is omitted because of the sparse table. By using a 250-second time step, this algorithm reduced computation time by 95.6% over the brute force method that generated the truth table.

Conclusions

This paper presents a very powerful method to rapidly determine the rise-set times of satellite-satellite and satellite-ground station visibility periods, with the

TABLE 7. One Day Rise-Set Summary for Satellite #2 vs Satellite #3 (oblate Earth)

Parabolic Blending		Angles Simulation		Absolute Difference	
Rise	Set	Rise	Set	Rise	Set
	2997.8		2997.8		0.0
5924.0	8944.6	5924.0	8944.7	0.0	0.1
11427.1	14479.2	11427.2	14479.2	0.1	0.0
16869.0	19941.6	16869.0	19941.6	0.0	0.0
22288.7	25375.1	22288.6	25377.1	0.1	0.0
27697.0	30793.4	27697.0	30793.5	0.0	0.1
33098.7	36202.6	33098.6	36202.6	0.1	0.0
38495.8	41605.7	38495.8	41605.7	0.0	0.0
43889.9	47004.5	43889.9	47004.5	0.0	0.0
49281.7	52400.1	49281.6	52400.1	0.1	0.0
54671.6	57793.4	54671.6	57793.4	0.0	0.0
60060.2	63184.7	60060.2	63184.7	0.0	0.0
65447.7	68574.6	65447.7	68574.6	0.0	0.0
70834.3	73963.2	70834.3	73963.2	0.0	0.0
76220.1	79350.8	76220.1	79350.8	0.0	0.0
81605.3	84737.5	81605.2	84737.5	0.1	0.0

TABLE 8. One Day Rise-Set Summary for Satellite #3 vs USAFA (125 second step size)

Parabolic Blending		Angles Simulation		Absolute Difference	
Rise	Set	Rise	Set	Rise	Set
366.3	793.8	366.4	793.4	0.1	0.4
5973.7	6041.8	5972.3	6044.8	1.4	3.0
39460.4	39950.0	39461.0	39949.4	0.6	0.6
44907.3	45293.0	44907.2	45291.8	0.1	1.2
86361.1		86361.2		0.1	

line-of-sight corrected for an oblate Earth. The extensive test results demonstrate the completeness of this routine, which is free of orbital restrictions and transcendental equations. Because the ephemeris generation and rise-set determination are distinct problems, this allows the user to tabulate $\psi(t)$ to any desired accuracy from existing software tools. Thus, if one wishes to perform parametric studies using satellite communication links as the performance index, perhaps generating a J_2-based $\psi(t)$ reference file might suffice. These results give the space-mission designer a first approximation about the viewing payoff of various satellite deployment strategies as well as the demand a vehicle places on a ground station. Also for programs requiring precise knowledge about viewing times, the designer can generate a $\psi(t)$ table based on numerical methods using a very detailed orbital motion model. For platforms with rapidly varying trajectories, the user can generate a very dense data set to accomplish curve modeling, provided the motion doesn't become too discontinuous, especially

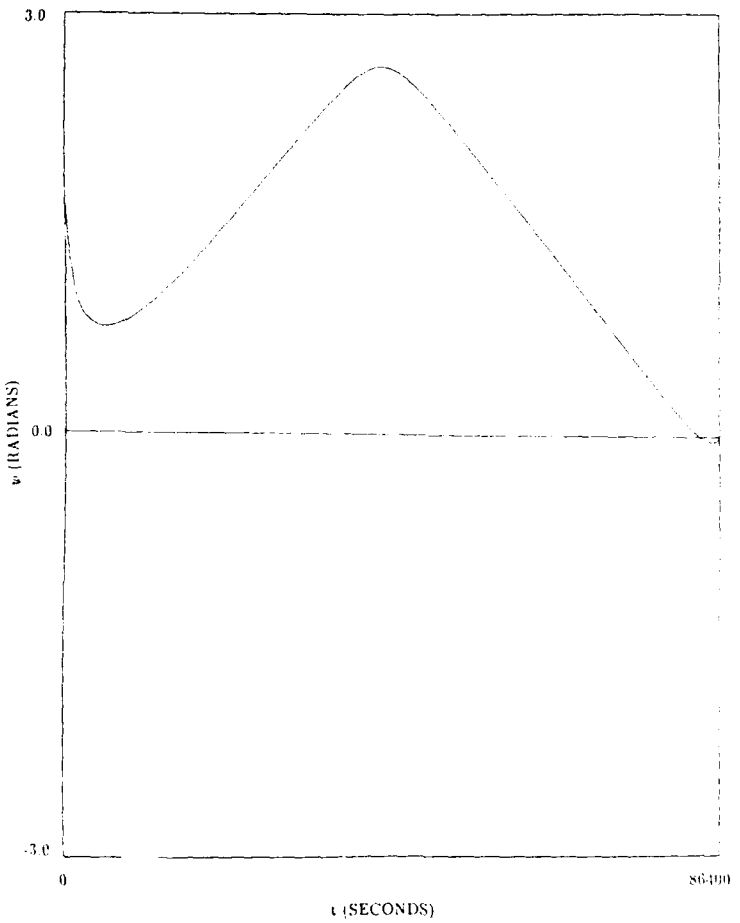

FIG. 4. Visibility Waveform for Satellite #1 versus Satellite #2.

near viewing entrance or exit. This logic can also be integrated onboard the satellite computer to support autonomous operations; the computer generates a rise-set table for a target set and then activates various instruments and operating modes once a target enters the visibility window. This routine can be tailored to process range restricted viewing links, as demonstrated by Negron, et al. [6].

Appendix A

Algorithm for Rise-Set Determination

1. Create a reference file of m ordered pairs, $(t_1, \psi_1) \ldots (t_m, \psi_m)$, where the t_i are times and the ψ_i are the associated visibility angles (250 second time intervals suggested, spacing need not be constant). The variable m should have a minimum value of 2.

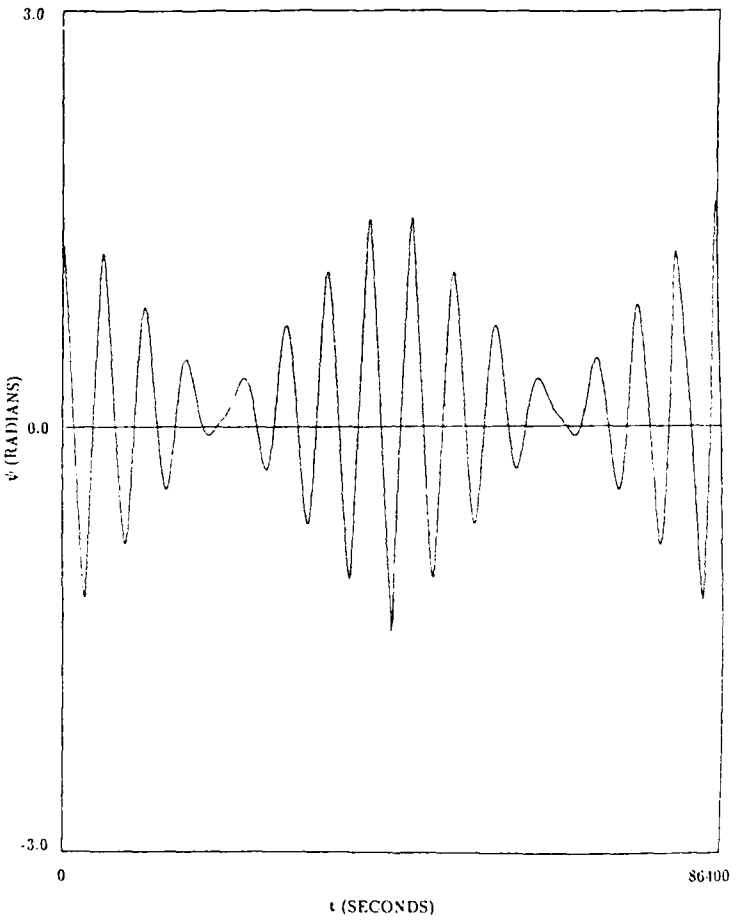

FIG. 5. Visibility Waveform for Satellite #1 versus Satellite #3.

2. Repeat the endpoints by assigning $(t_0, \psi_0) = (t_1, \psi_1)$ and $(t_{m+1}, \psi_{m+1}) = (t_m, \psi_m)$.
3. Begin a loop with i as the index running from 1 to $m - 1$:
   a. Use the angles ψ_{i-1}, ψ_i, ψ_{i+1}, and ψ_{i+2} to compute $\alpha_{\psi 0}$, $\alpha_{\psi 1}$, $\alpha_{\psi 2}$, and $\alpha_{\psi 3}$.
   b. Solve the cubic $C_\psi(T)$ equation for real roots (T_1, T_2, T_3) in the interval $0 \le T < 1$.
      Rescale these unitized roots (if any) to time as follows:
      (1) Use the times t_{i-1}, t_i, t_{i+1}, and t_{i+2} to compute α_{t0}, α_{t1}, α_{t2}, and α_{t3}.
      (2) Compute rescaled time = $C_t(T_{ROOT})$.
      (3) Determine if this is a rise or set time by incrementing T by some δ and solve for $C_\psi(T_{ROOT} + \delta)$. If C_ψ is positive, then $C_t(T_{ROOT})$ is a rise time, otherwise it's a set time.
   c. Return to Step 3.

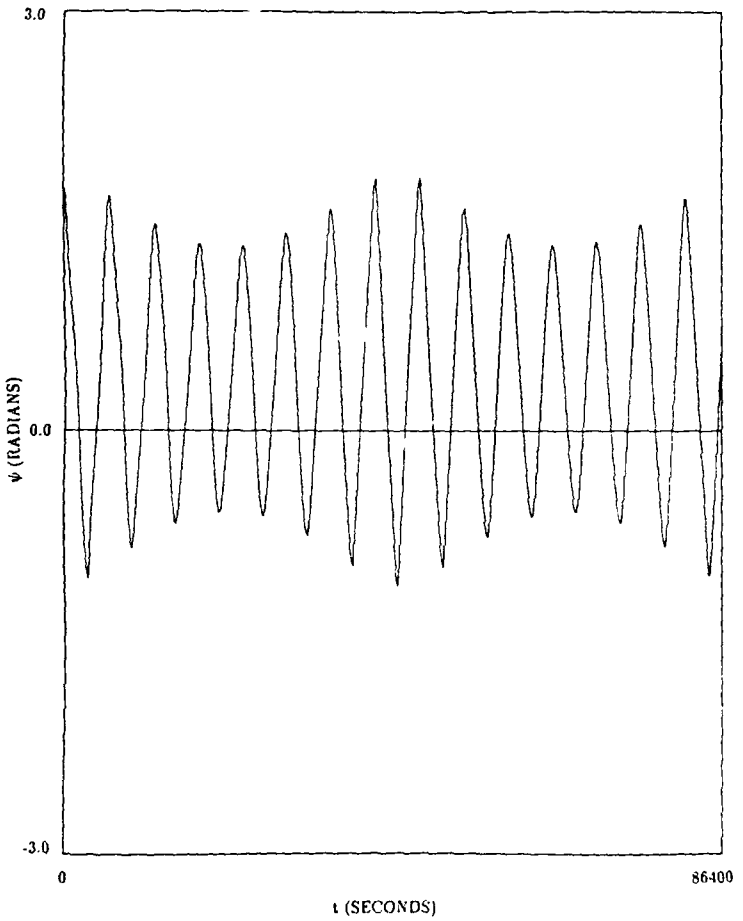

FIG. 6. Visibility Waveform for Satellite #1 versus Satellite #4.

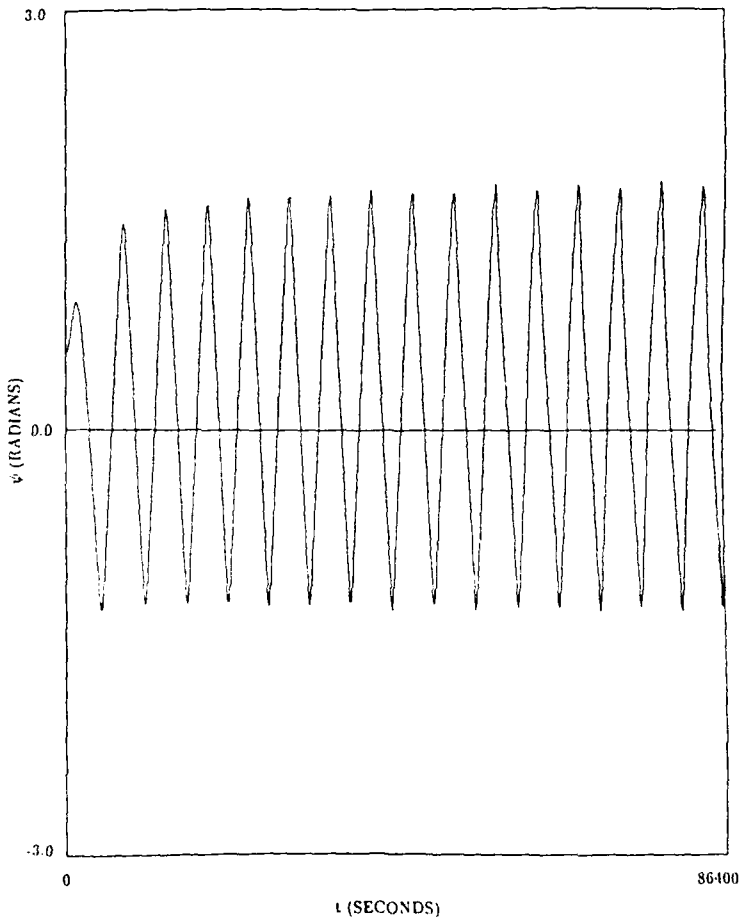

FIG. 7. Visibility Waveform for Satellite #2 versus Satellite #3.

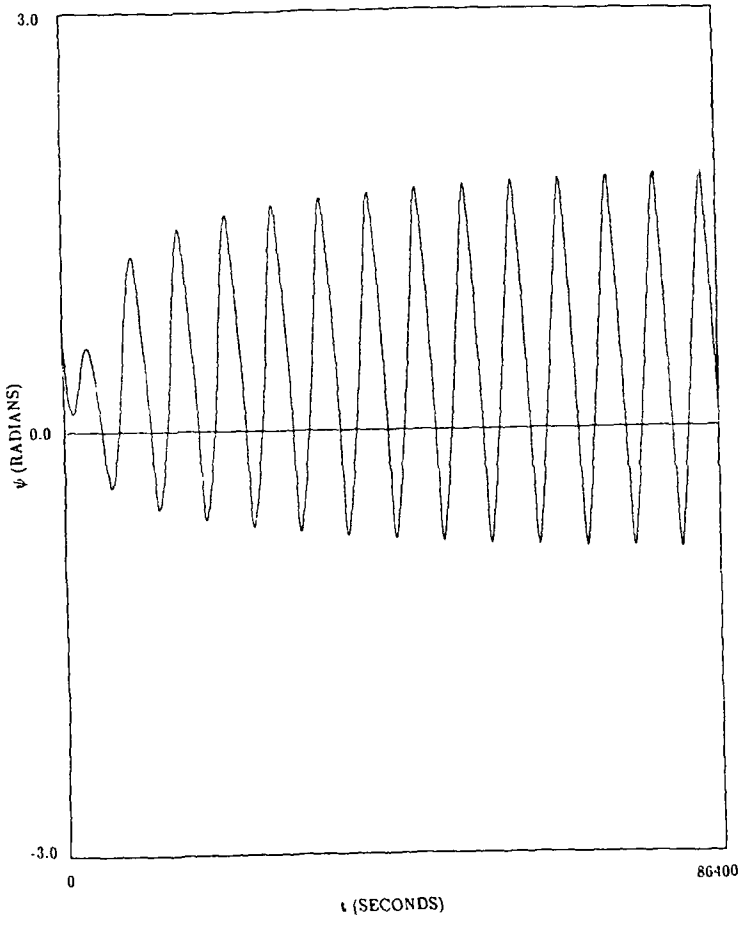

FIG. 8. Visibility Waveform for Satellite #2 versus Satellite #4.

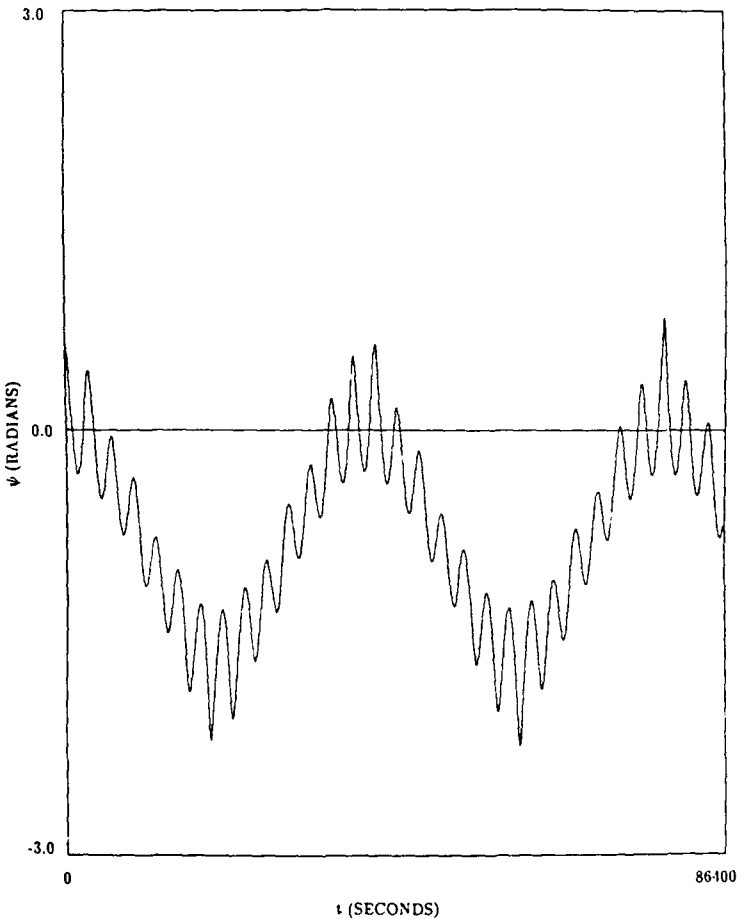

FIG. 9. Visibility Waveform for Satellite #3 versus Satellite #4.

References

[1] ESCOBAL, P. R. "Rise and Set Time of a Satellite about an Oblate Planet," *AIAA Journal*, Vol. 1, No. 10, October 1963, pp. 2306–2310.

[2] LAWTON, J. A. "Numerical Method for Rapidly Determining Satellite-Satellite and Satellite-Ground Station In-View Periods," *Journal of Guidance, Navigation, and Control*, Vol. 10, January-February 1987, pp. 32–36.

[3] OVERHAUSER, A.W. "Analytic Definition of Curves and Surfaces by Parabolic Blending," Ford Motor Company Scientific Laboratory, Technical Report No. SL68-40, May 8, 1968.

[4] BREWER, J. A., and ANDERSON, D. C. "Visual Interaction with Overhauser Curves and Surfaces," *Computer Graphics*, Vol. 11, 1978 (SIGGRAPH 77), pp. 132–137.

[5] ESCOBAL, P. R. *Methods of Orbit Determination*, Robert E. Krieger Publishing Company, Huntington, New York, 1965, pp. 26–29 and 360–369.

[6] NEGRON, JR., D., ALFANO, S., and WRIGHT, III, D. "The Method of Ratios," *Journal of the Astronautical Sciences*, Vol. 40, No. 2, April-June 1992, pp. 297–309.